

A facile one-pot ultrasound-assisted green synthesis of tetrahydrobenzo[b]pyrans catalyzed by gold nanoparticles supported on thiol-functionalized reduced graphene oxide

Hossein Naeimi¹ · Maryam Farahnak Zarabi¹

Received: 25 November 2017 / Accepted: 17 January 2018
© Springer Science+Business Media B.V., part of Springer Nature 2018

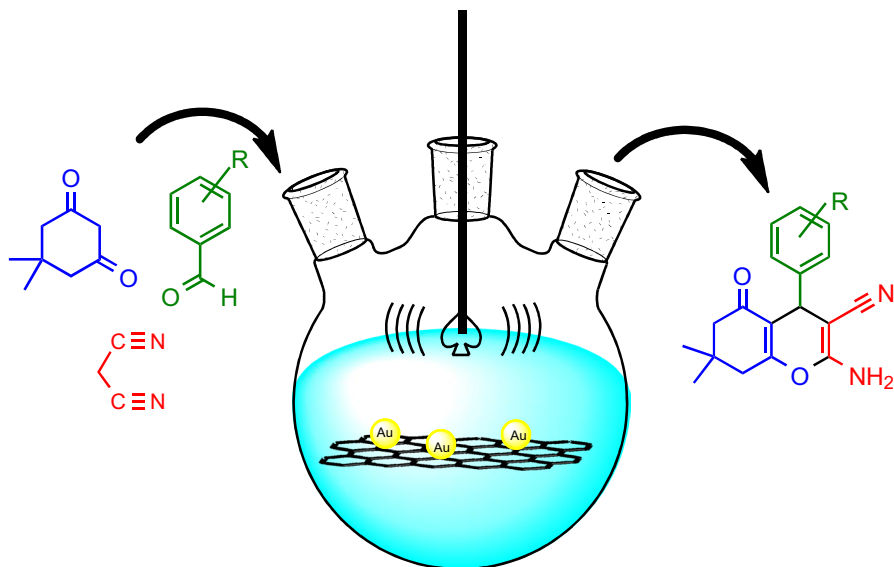
Abstract A convenient one-pot protocol was explored for the preparation of tetrahydrobenzo[b]pyrans. This reaction was carried out through a three-component condensation reaction of malononitrile, dimedone and aldehyde in the presence of gold nanoparticles on thiol-functionalized reduced graphene oxide as a catalyst in water under ultrasound irradiation. The pure products were obtained in high yields and short reaction times. Also, this catalyst can be easily separated from the reaction and recycled six times without activity loss.

Electronic supplementary material The online version of this article (<https://doi.org/10.1007/s11164-018-3303-6>) contains supplementary material, which is available to authorized users.

✉ Hossein Naeimi
naeimi@kashanu.ac.ir

¹ Department of Organic Chemistry, Faculty of Chemistry, University of Kashan, Kashan 87317, Islamic Republic of Iran

Graphical Abstract



Keywords Ultrasound · Graphene oxide · Gold nanoparticles · Tetrahydrobenzo[b]pyran

Introduction

The synthesis of tetrahydrobenzo[b]pyran derivatives is important because of their wide range of applications. These molecules are commonly employed in many fields such as anticoagulant, anticancer, spasmolytic, antibacterial, anti-anaphylactic activity, and diuretic [1–6]. These heterocycles are usually synthesized using dimedone, aromatic aldehydes and malononitrile in the presence of various catalysts. A number of catalysts have been reported for the synthesis of 4H-benzo-[b]-pyrans such as ionic liquid [7], hexadecyldimethylbenzyl ammonium bromide [8], tetrabutyl ammonium bromide (TBAB) [9], sodium selenite [10], fluoride ion [11], molecular iodine [12], Amberlite IRA-40 [13], ZnO-Zeolite [14], and nanoparticles [15–17]. Some of these protocols have their own merits and demerits, such as low yields of products, long reaction times, harsh reaction conditions and tedious work-ups leading to the generation of large amounts of toxic waste. Therefore, a great deal of effort is being directed to developing an efficient catalytic system for the synthesis of 4H-pyrans.

Graphene is a typical support for the preparation of heterogeneous catalysts, which has attracted much attention in recent years. Graphene sheets which give remarkable thermal, electronic, and mechanical properties, have a variety of applications including nanocomposites, sensors, supercapacitors, batteries, and hydrogen

storage [18–24]. Graphene oxide (GO) containing oxygen-rich functional groups, such as epoxide, hydroxyls, and carboxylic acids, provide anchors for further chemical modifications, and can be used as an excellent support for heterogeneous catalysts in organic synthesis because of wonderful characteristics such as easy synthesis, chemical and thermal stability, and high specific surface area [22–29]. The impact in the association of high-surface-area inorganic supports with metallic nanoparticles producing nanocomposites with better dispersity and stability of the particles and recycling properties of the catalyst [30]. One way to increase the surface area is to reduce the particle size [31]. Among nanoparticles, AuNPs are of great interest because of their remarkable properties and have been widely used in catalysis, optics, and nanobiotechnology [32]. Recently, several gold heterogeneous catalysts were successfully used in A³-coupling [33], oxidation of secondary amines [34], alcohols [35] and carbon monoxide [36], Sonogashira [37] and Suzuki [38] reactions, etc. These systems were used either in required drastic reaction conditions or in toxic solvents. Therefore, the development of highly efficient gold catalysts in environmentally friendly media is favored.

Sonochemical synthesis is a facile, rapid, powerful and environmentally friendly technique, which has recently been applied to the synthesis of organic compounds [39]. Ultrasonic irradiation formed bubbles, and their collapse generated localized hot spots with very short life-times and extremely high temperatures and pressures (up to 5000 °C and 2000 atm) [40]. An ultrasound approach is an important technique with prominent features including increased reaction rates, high yields, easier manipulation, mild reaction conditions, and waste minimization compared with traditional methods [41, 42]. Ultrasound is a more convenient method for green and sustainable synthetic processes [43].

In this article, we decided to investigate the application of gold nanoparticles on thiol-functionalized reduced graphene oxide (RGO-Pr-SH@AuNPs) as a catalyst for the synthesis of tetrahydrobenzo[b]pyrans in water media under ultrasound irradiation.

Experimental

Materials and apparatus

The chemicals were purchased from Fluka and Merck and used without purification. FT-IR spectra were obtained as KBr pellets on a Perkin-Elmer 781 spectrophotometer and on an impact 400 Nicolet FT-IR spectrophotometer. ¹H NMR was recorded in DMSO-d₆ and CDCl₃ solvents on a Bruker DRX-400 spectrometer with tetramethylsilane as internal reference. A Bandelin ultrasonic HD 3200 with a 6-mm-diameter model KE 76 probe was used to generate ultrasonic irradiation and homogenize the reaction mixture. The piezoelectric crystals in this kind of probe normally work at approximately 700 kHz, by use of appropriate clamps. However, the output frequency of piezoelectric crystals was controlled and reduced to 20 kHz in the reaction mixture. The elemental analyses (C, H, N) were obtained from a Carlo ERBA Model EA 1108 analyzer. XRD patterns were obtained by an X'PertPro (Philips)

instrument with 1.54 Å wavelengths of the X-ray beam and Cu anode material, at a scanning speed of 2° min^{-1} from 10° to 80° (2θ). Thermogravimetric analysis (TGA) was performed on a Mettler TA4000 system TG-50 at a heating rate of 10 K min^{-1} under N_2 atmosphere. The surface morphology of the supported catalyst was studied using field-emission scanning electron microscopy (FE-SEM). FE-SEM and elemental analysis were carried out using a Jeol SEM instrument (VEGA/TESCAN) combined with an INCA instrument for energy-dispersive X-ray spectroscopy (EDS), with a scanning electron electrode at 15 kV. The AFM image of the catalysts was investigated using scanning probe microscopy (SPM-9600; Shimadzu). Transmission electron microscopy (TEM) analyses were performed using a JEOL-JEN 2010 transmission electron microscope operated at an accelerating voltage of 200 kV. The measurements of Raman spectroscopy were recorded using a Thermo Nicolet Almega Dispersive Raman Spectrometer. Also, elemental analyses of the catalyst with inductively coupled plasma atomic emission spectroscopy were obtained from an ICP-OES simultaneous instrument (VISTA-PRO). Melting points were measured with a Yanagimoto micro-melting point apparatus. The purity determination of the substrates and reaction monitoring were accomplished by TLC on silica-gel polygram SILG/UV 254 plates (Merck).

Preparation of catalyst

Preparation of graphene oxide (GO)

The GO nanosheets were synthesized by a modified Hummer's method. Typically, a 1000-mL round-bottom flask equipped with a magnetic bar and containing a mixture of 5.0 g of natural graphite powder, 2.5 g of sodium nitrate and 115 mL of sulfuric acid (98%) was placed in an ice bath. Then, 15.0 g of potassium permanganate were slowly added to the obtained solution and stirred for 2 h. The solution was then placed in a water bath (35°C) and stirred for 30 min. Then, deionized water (230 mL) was added slowly with a solution temperature of about 98°C and stirred for 15 min. Afterward, 700 mL of deionized water and 50 mL of H_2O_2 (30%) were added to the solution. The resulting materials were filtered and washed several times by dilute HCl (5%) and deionized water. Then, GO powder was obtained after drying for 12 h at 60°C under vacuum. The GO powder was dispersed in distilled water to give a concentration of 0.5 mg mL^{-1} and exfoliated by ultrasonication to obtain GO nanosheets.

Preparation of thiol-functionalized GO nanosheets

GO nanosheets (0.3 g) were suspended in 20 mL toluene using an ultrasonic probe, and (3-mercaptopropyl)trimethoxysilane (1.0 mL) was added to the mixture, which was then refluxed and stirred for 48 h under nitrogen atmosphere. After completion of the reaction, the functionalized GO nanosheets were washed with toluene and absolute ethanol and dried under vacuum overnight. The synthesis of thiol-functionalized GO was confirmed by IR, TGA, and elemental analysis.

Preparation of RGO-Pr-SH@AuNPs

Thiol-functionalized GO nanosheets (0.2 g in 10.0 mL) were mixed with 0.2 g aqueous HAuCl_4 and placed in an ultrasonic (30 kHz) for 30 min to well disperse. In the subsequent step, a freshly prepared solution of NaBH_4 (1.0 M) was added. The mixture was stirred at room temperature for 8 h. The resulting mixture was filtered and washed with ethanol/water and dried under vacuum overnight. The RGO-Pr-SH@AuNPs catalyst was investigated by IR, ICP, TGA, XRD, FE-SEM, and AFM.

General procedure for the preparation of tetrahydrobenzo[b]pyran catalyzed by RGO-Pr-SH@AuNPs under ultrasound irradiation

A mixture of dimedone (1 mmol), malononitrile (1 mmol), aldehyde (1 mmol), and catalyst RGO-Pr-SH@AuNPs (3 mg, 0.22 mol% Au) in water (2 mL) was sonicated at 40 kHz at room temperature for the appropriate time. The progress of the reaction was monitored by thin layer chromatography (TLC) and used *n*-hexane/ethyl acetate as an eluent. After completion of the reaction, the product was dissolved in hot ethanol, and, subsequently, the catalyst was filtered under reduced pressure using a vacuum pump over sintered glass. The solvent was eliminated under vacuum to give the corresponding product. The products were confirmed by spectral and physical data and were compared with authentic samples [44–47]. The recovered catalyst was washed with EtOH and dried at 80 °C in vacuum. The catalyst was recycled six times without any significant changes observed in the yields and reaction times.

2-amino-7,7-dimethyl-5-oxo-4-phenyl-5,6,7,8-tetrahydro-4H-chromene-3-carbonitrile (1) mp: 229–232 °C (lit. [44]: 231–233 °C); IR (KBr, cm^{-1}): 3395, 3324, 3211, 2962, 2198, 1679, 1660, 1602, 1369, 1213. ^1H NMR (400 MHz, $\text{DMSO}-d_6$): δ = 0.94 (s, 3H), 1.03 (s, 3H), 2.08 (d, 2J = 16.0 Hz, 1H), 2.24 (d, 2J = 16.0 Hz, 1H), 2.49 (s, 2H), 4.16 (s, 1H), 6.99 (s, 2H), 7.13 (d, 3J = 8.0 Hz, 2H), 7.15–7.19 (m, 1H), 7.27 (t, 3J = 8.0 Hz, 2H).

2-amino-4-(4-(dimethylamino)phenyl)-7,7-dimethyl-5-oxo-5,6,7,8-tetrahydro-4H-chromene-3-carbonitrile (2) mp: 213–215 °C (lit. [45]: 211–214 °C); IR (KBr, cm^{-1}): 3381, 3318, 3207, 2959, 2190, 1679, 1655, 1608, 1366, 1213. ^1H NMR (400 MHz, $\text{DMSO}-d_6$): δ = 0.94 (s, 3H), 1.02 (s, 3H), 2.07 (d, 2J = 16.0 Hz, 1H), 2.23 (d, 2J = 16.0 Hz, 1H), 2.49 (s, 2H), 2.83 (s, 6H), 4.03 (s, 1H), 6.62 (d, 3J = 8.0 Hz, 2H), 6.89 (s, 2H), 6.92 (d, 3J = 8.0 Hz, 2H).

2-amino-4-(2-chlorophenyl)-7,7-dimethyl-5-oxo-5,6,7,8-tetrahydro-4H-chromene-3-carbonitrile (3) mp: 213–215 °C (lit. [44]: 209–211 °C); IR (KBr, cm^{-1}): 3217, 2954, 2193, 1710, 1612. ^1H NMR (400 MHz, $\text{DMSO}-d_6$): δ = 1.06 (s, 3H), 1.07 (s, 3H), 2.16 (d, 2J = 16.0 Hz, 1H), 2.23 (d, 2J = 16.0 Hz, 1H), 2.28–2.32 (m, 2H), 4.47 (s, 1H), 6.95 (m, 1H), 7.24 (m, 2H), 7.46 (m, 1H).

2-amino-4-(3-chlorophenyl)-7,7-dimethyl-5-oxo-5,6,7,8-tetrahydro-4H-chromene-3-carbonitrile (4) mp: 225–228 °C (lit. [44]: 224–226 °C); IR (KBr, cm^{-1}): 3236, 3163, 2955, 2117, 1704, 1617, 1473. ^1H NMR (400 MHz, CDCl_3): δ = 1.07 (s, 3H), 1.15 (s, 3H), 2.29–2.32 (m, 3H), 2.46 (d, 2J = 16.4 Hz, 1H), 4.34 (s, 1H), 7.11(m, 1H), 7.18 (m, 3H), 7.48 (s, 2H).

2-amino-4-(4-chlorophenyl)-7,7-dimethyl-5-oxo-5,6,7,8-tetrahydro-4H-chromene-3-carbonitrile (5) mp: 208–210 °C (lit. [44]: 208–210 °C); IR (KBr, cm^{-1}): 3380, 3323, 3183, 2959, 2188, 1675, 1635, 1603, 1365, 1216. ^1H NMR (400 MHz, $\text{DMSO}-d_6$): δ = 0.93 (s, 3H), 1.02 (s, 3H), 2.08 (d, 2J = 16.4 Hz, 1H), 2.24 (d, 2J = 16.4 Hz, 1H), 2.49 (s, 2H), 4.18 (s, 1H), 7.07 (s, 2H), 7.15 (d, 3J = 8.4 Hz, 2H), 7.33 (d, 3J = 8.4 Hz, 2H).

2-amino-4-(2,4-dichlorophenyl)-7,7-dimethyl-5-oxo-5,6,7,8-tetrahydro-4H-chromene-3-carbonitrile (6) mp: 118–119 °C (lit. [46]: 115–117 °C); IR (KBr, cm^{-1}): 3361, 3320, 3158, 2964, 2192, 1684, 1658, 1604, 1366, 1216. ^1H NMR (400 MHz, $\text{DMSO}-d_6$): δ = 0.96 (s, 3H), 1.03 (s, 3H), 2.07 (d, 2J = 16.0 Hz, 1H), 2.24 (d, 2J = 16.0 Hz, 1H), 2.45 (s, 2H), 4.67 (s, 1H), 7.11 (s, 2H), 7.21 (d, 3J = 8.4 Hz, 1H), 7.35 (d, 3J = 8.4 Hz, 1H), 7.52 (s, 1H).

2-amino-4-(3-bromophenyl)-7,7-dimethyl-5-oxo-5,6,7,8-tetrahydro-4H-chromene-3-carbonitrile (7) mp: 282–285 °C (lit. [44]: 287–289 °C); IR (KBr, cm^{-1}): 3343, 3303, 3167, 2962, 2191, 1683, 1657, 1604, 1369, 1214. ^1H NMR (400 MHz, $\text{DMSO}-d_6$): δ = 0.95 (s, 3H), 1.03 (s, 3H), 2.11 (d, 2J = 16.0 Hz, 1H), 2.25 (d, 2J = 16.0 Hz, 1H), 2.52 (s, 2H), 4.19 (s, 1H), 7.10 (s, 2H), 7.15 (d, 3J = 8.0 Hz, 1H), 7.26 (t, 3J = 8.0 Hz, 1H), 7.29 (s, 1H), 7.38 (d, 3J = 8.0 Hz, 1H).

2-amino-4-(4-bromophenyl)-7,7-dimethyl-5-oxo-5,6,7,8-tetrahydro-4H-chromene-3-carbonitrile (8) mp: 205–207 °C (lit. [44]: 203–205 °C); IR (KBr, cm^{-1}): 3389, 3320, 3186, 2960, 2189, 1679, 1637, 1604, 1365, 1214. ^1H NMR (400 MHz, $\text{DMSO}-d_6$): δ = 0.94 (s, 3H), 1.02 (s, 3H), 2.09 (d, 2J = 16.0 Hz, 1H), 2.24 (d, 2J = 16.0 Hz, 1H), 2.49 (s, 2H), 4.17 (s, 1H), 7.06 (s, 2H), 7.10 (d, 3J = 8.0 Hz, 2H), 7.47 (d, 3J = 8.0 Hz, 2H).

2-amino-4-(4-fluorophenyl)-7,7-dimethyl-5-oxo-5,6,7,8-tetrahydro-4H-chromene-3-carbonitrile (9) mp: 202–205 °C (lit. [44]: 210–212 °C); IR (KBr, cm^{-1}): 3229, 2957, 2204, 1686, 1660, 1602, 1362, 1222. ^1H NMR (400 MHz, CDCl_3): δ = 0.99 (s, 3H), 1.11 (s, 3H), 2.15–2.27 (m, 2H), 2.47 (s, 2H), 4.73 (s, 1H), 6.89–6.97 (m, 4H), 7.17–7.25 (s, 2H).

2-amino-4-(4-methylphenyl)-7,7-dimethyl-5-oxo-5,6,7,8-tetrahydro-4H-chromene-3-carbonitrile (10) mp: 215–218 °C (lit. [44]: 217–219 °C); IR (KBr, cm^{-1}): 3392, 3321, 3210, 2962, 2192, 1682, 1655, 1603, 1366, 1213. ^1H NMR (400 MHz, CDCl_3): δ = 0.96 (s, 3H), 1.07 (s, 3H), 2.22 (s, 3H), 2.25–2.42 (m, 4H), 5.04 (s, 1H), 6.99 (d, 3J = 5.6 Hz, 2H), 7.21 (d, 3J = 5.6 Hz, 2H), 7.59 (s, 2H).

2-amino-4-(3-methoxyphenyl)-7,7-dimethyl-5-oxo-5,6,7,8-tetrahydro-4H-chromene-3-carbonitrile (11) mp: 183–187 °C (lit. [44]: 190–192 °C); IR (KBr, cm^{-1}): 3242, 3160, 2957, 2174, 1704, 1614. ^1H NMR (400 MHz, CDCl_3): δ = 1.07 (s, 3H), 1.14 (s, 3H), 2.29–2.33 (s, 2H and d, 2J = 16.0 Hz, 1H), 2.45 (d, 2J = 16.0 Hz, 1H), 3.76 (s, 3H), 4.34 (s, 1H), 6.73–6.76 (m, 2H), 6.79 (d, 3J = 8.0 Hz, 1H), 7.18 (t, 3J = 8.0 Hz, 1H), 8.15 (s, 2H).

2-amino-4-(4-methoxyphenyl)-7,7-dimethyl-5-oxo-5,6,7,8-tetrahydro-4H-chromene-3-carbonitrile (12) mp: 190–193 °C (lit. [44]: 193–195 °C); IR (KBr, cm^{-1}): 3276, 3206, 3070, 2956, 2183, 1702, 1644, 1608, 1482, 1223. ^1H NMR (400 MHz, CDCl_3): δ = 0.95 (s, 3H), 1.06 (s, 3H), 2.12–2.31 (m, 4H), 3.68 (s, 3H), 5.03 (s, 1H), 6.72 (d, 3J = 6.8 Hz, 2H), 7.25 (d, 3J = 6.8 Hz, 2H), 7.90 (s, 2H).

2-amino-4-(5-bromo-2-hydroxyphenyl)-7,7-dimethyl-5-oxo-5,6,7,8-tetrahydro-4H-chromene-3-carbonitrile (13) mp: 190–193 °C; IR (KBr, cm^{-1}): 3362, 3200, 3101, 2955, 2214, 1688, 1621. ^1H NMR (400 MHz, $\text{DMSO}-d_6$): δ = 0.90 (s, 3H), 1.01 (s, 3H), 2.04 (d, 2J = 16.0 Hz, 1H), 2.23 (d, 2J = 15.6 Hz, 1H), 2.36 (d, 2J = 16.0 Hz, 1H), 2.47 (d, 2J = 15.6 Hz, 1H), 4.77 (s, 1H), 6.64 (d, 3J = 8.4 Hz, 1H), 6.97 (s, 1H), 7.06 (d, 3J = 8.4 Hz, 1H), 9.68 (s, 1H). Anal. Calcd. for $\text{C}_{18}\text{H}_{17}\text{BrN}_2\text{O}_3$: C, 55.54; H, 4.40; N, 7.20. Found: C, 55.62; H, 4.57; N, 7.41.

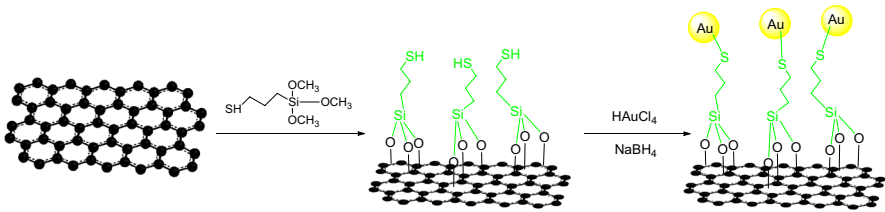
2-amino-7,7-dimethyl-4-(5-methylfuran-2-yl)-5-oxo-5,6,7,8-tetrahydro-4H-chromene-3-carbonitrile (14) mp: 201–203 °C (lit [47]: 205–207 °C); IR (KBr, cm^{-1}): 3383, 3321, 3207, 2961, 2198, 1662, 1602, 1373, 1214. ^1H NMR (400 MHz, CDCl_3): δ = 1.07 (s, 3H), 1.12 (s, 3H), 1.59 (s, 3H), 2.27 (s, 2H), 2.43 (s, 2H), 4.23 (s, 1H), 6.90–6.91 (m, 1H), 6.99 (s, 2H), 7.13–7.14 (m, 1H).

2-amino-7,7-dimethyl-5-oxo-4-(thiophen-2-yl)-5,6,7,8-tetrahydro-4H-chromene-3-carbonitrile (15) mp: 211–214 °C (lit [47]: 208–210 °C); IR (KBr, cm^{-1}): 3426, 3284, 3207, 2958, 2214, 1688, 1617, 1480, 1368, 1228. ^1H NMR (400 MHz, CDCl_3): δ = 0.92 (s, 3H), 0.94 (s, 3H), 2.35 (s, 2H), 2.44 (s, 2H), 4.21 (s, 1H), 7.53–7.55 (m, 2H), 7.71–7.72 (m, 1H).

Results and discussion

Preparation and characterization of the catalyst

The process for the preparation of the RGO-Pr-SH@AuNPs catalyst is described in Scheme 1. GO nanosheets were prepared using a modified Hummer's method, and subsequently functionalized with thiol. Gold nanoparticles were deposited on the surface of the reduced GO (RGO) through simultaneous chemical reduction of HAuCl_4 and GO with NaBH_4 . In recent years, mercapto groups have been used as stabilizers of gold nanoparticles (due to the high affinity of Au and S), which limit the mobility and aggregation of the gold nanoparticles on surfaces, and to obtain a



Scheme 1 Preparation of RGO-Pr-SH@AuNPs nanocatalyst

high loading of AuNPs on the surface. After successful preparation of the RGO-Pr-SH@AuNPs, the catalyst was characterized by ICP, TGA, FT-IR, XRD, AFM, and FESEM.

Figure 1a–d shows the FT-IR spectra of graphite, GO, GO-Pr-SH, and RGO-Pr-SH@AuNPs, respectively. The FT-IR spectrum of graphite powder shows peaks characteristic of C=C groups at 1573 cm^{-1} , but the peak is not sharp (Fig. 1a). Figure 1b shows the FT-IR spectrum of GO powder. The absorption band at 1578 cm^{-1} is related to C=C double bonds and this peak is sharper than for graphite due to the asymmetry of the GO. The absorption peaks at 1030 , 1720 and 3400 cm^{-1} are assigned to the C–O, carbonyl, and hydroxyl stretching modes of functional groups attachment to GO, respectively. The numerous functional groups on the GO provide active sites for the bonding between the GO sheets and silane compounds. Figure 1c shows the FT-IR spectrum of the thiol-functionalized GO. The FT-IR absorption peak at 1110 cm^{-1} represents the Si–O–C bond that clearly shows the grafting step. The vibrational bands at 2924 and 2853 cm^{-1} are attributed to aliphatic CH_2 groups

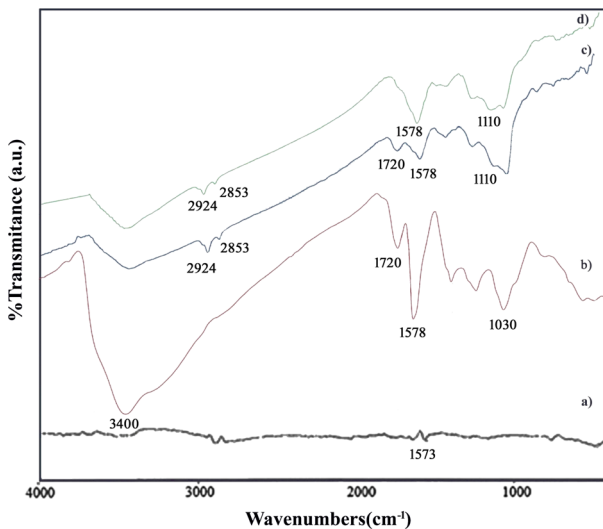


Fig. 1 FT-IR spectra of (a) graphite, (b) GO, (c) GO-Pr-SH, and (d) RGO-Pr-SH@AuNPs

of (3-mercaptopropyl) trimethoxysilane, which confirms the attachment of thiol groups to the GO through chemical bonding. In the FT-IR spectrum of the RGO-Pr-SH@AuNPs, the peak of the carbonyl group has disappeared, which confirms the chemical reduction of GO with NaBH_4 (Fig. 1d). In addition, the absorption band at 1578 cm^{-1} shows that, after chemical reduction, the RGO is still in flake-like sheets. Because the SH and OH peaks are broad, the IR band of SH is not clear.

Figure 2 shows XRD patterns of graphite, GO and RGO-Pr-SH@AuNPs, respectively. The XRD pattern of graphite (Fig. 2a) exhibits a peak at approximately $2\theta = 26.5^\circ$ corresponding to the interlayer spacing (d -spacing = 0.335 nm). In Fig. 2b, GO exhibits a broad diffraction peak at about $2\theta = 26.5^\circ$ and a peak at $2\theta = 12^\circ$. The interlayer spacing (d -spacing) of GO was calculated to be 0.78 nm which revealed the formation of oxygen-containing functional groups between the layers of the graphite. In Fig. 2c, well-defined peaks at 2θ values of 38.18° , 44.43° , 64.73° and 77.69° are assigned to face-centered cubic (fcc) bulk gold (111), (200), (220) and (311), respectively, which are in accordance to the standard values of gold. Also, the XRD pattern shows a broad diffraction peak at 25° which indicates the fully reduction of GO and the production of RGO nanosheets, so the XRD results further confirm the successful synthesis of RGO-Pr-SH@AuNPs nanocomposites. The Scherrer equation, $\tau = K\lambda/B \cos \theta$, was used to calculate the mean size of the gold nanoparticles, where τ is the average particle size, K is the shape factor (taken as 1.0), λ is the X-ray wavelength (0.154), β is the full width at half maximum (FWHM) intensity and θ is the Bragg angle. Thus, the size of gold nanoparticles was obtained to be about 21 nm, which is in good agreement with the TEM results.

Figure 3 shows the Raman spectra of the GO and RGO-Pr-SH@AuNPs. For the prepared samples, two bands are detected at ~ 1342 and $\sim 1598\text{ cm}^{-1}$, commonly

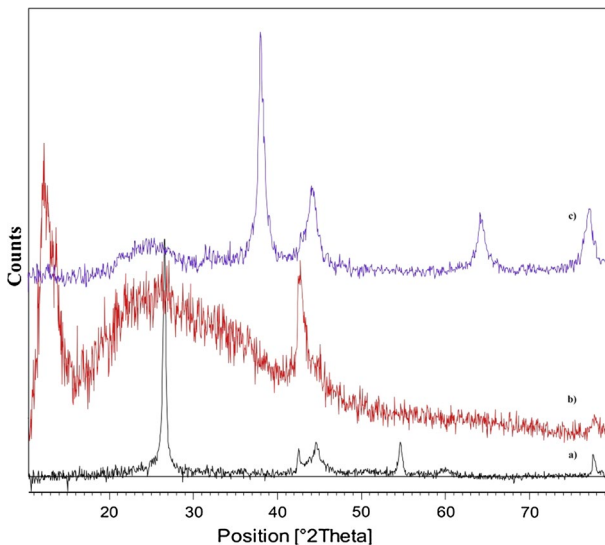


Fig. 2 XRD patterns of (a) graphite, (b) GO and (c) RGO-Pr-SH@AuNPs

denoted as the D band and the G-band of the carbon atoms [48]. The intensity ratio of the D band to the G band (I_D/I_G) of the GO and RGO-Pr-SH@AuNPs, increasing from 0.64 to 0.88, indicates the reduction of GO to RGO [49].

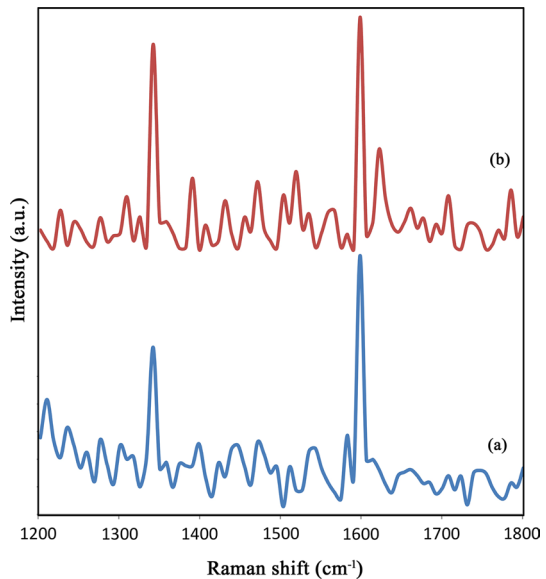
TGA of the RGO-Pr-SH@AuNPs nanocomposite is shown in Fig. 4. This catalyst shows a main weight loss between 180 and 660 °C attributed to the decomposition of covalently bonded organic groups from the RGO-Pr-SH@AuNPs. In addition, TGA analysis indicates that the prepared RGO-Pr-SH@AuNPs catalyst has good thermal stability up to 160 °C. The mass loss of 6.5% in the sample RGO-Pr-SH@AuNPs nanocomposite corresponds to 0.33 mmol g⁻¹ of the organosilane bound to the GO.

Figure 5a, b exhibit the FE-SEM images of GO and RGO-Pr-SH@AuNPs nanosheets, respectively. These images confirm the formation of the well-ordered two-dimensional and typical exfoliated nanosheets. Moreover, Fig. 5b of the RGO-Pr-SH@AuNPs nanocomposite reveals the presence of gold nanoparticles in the support with an average particle diameter of 15 ± 5 nm.

Figure 6 shows the TEM image of RGO-Pr-SH@AuNPs, indicating the size distribution of the uniformly dispersed gold nanoparticles. Moreover, TEM analysis presented the nanoparticle size as 20 ± 5 nm.

Figure 7 displays AFM images of GO and RGO-Pr-SH@AuNPs which are employed to observe the morphology of the GO nanosheets and measure their thickness. The AFM images of the GO and RGO-Pr-SH@AuNPs confirm the exfoliated nature of the graphene sheets. The images indicate that the GO nanosheet has an average thickness of 1 nm, corresponding to the presence of individual GO sheets in suspension (Fig. 7a). After simultaneous chemical reduction of HAuCl₄ and GO with NaBH₄, gold nanoparticles are deposited on the surface of the reduced GO (RGO) which was functionalized with thiol and the AFM analysis of the

Fig. 3 Raman spectra of (a) GO, (b) RGO-Pr-SH@AuNPs



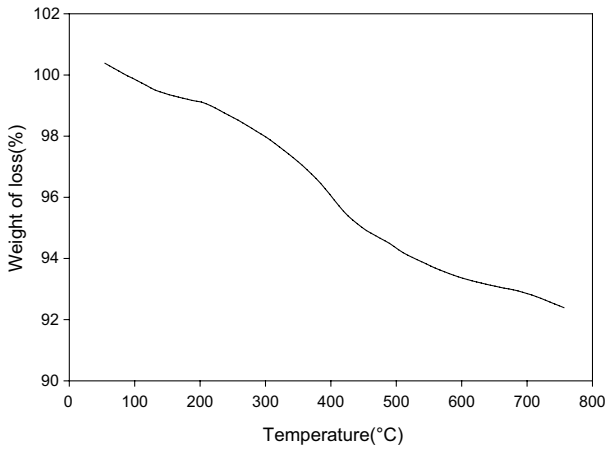


Fig. 4 TGA graph of RGO-Pr-SH@AuNPs

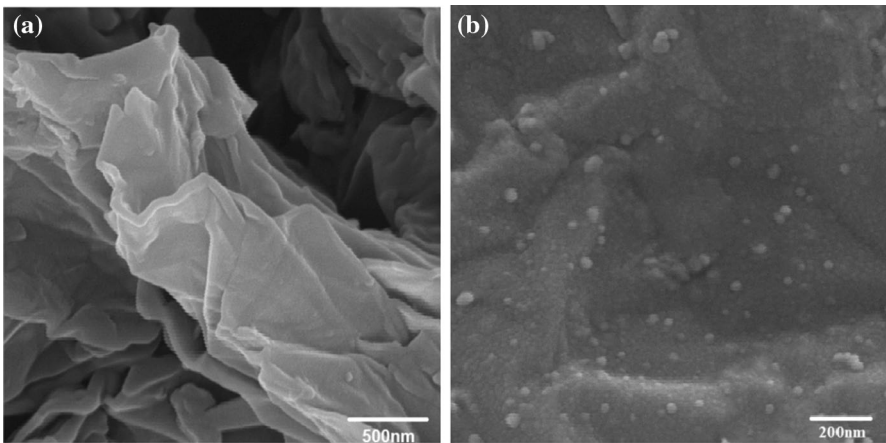
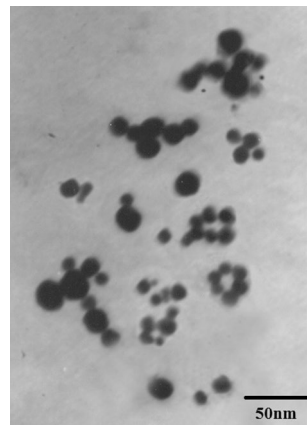


Fig. 5 FE-SEM images of **a** GO and **b** RGO-Pr-SH@AuNPs

RGO-Pr-SH@AuNPs is provided (Fig. 7b). A high density of the gold nanoparticles on graphene sheets is shown in all images. The AFM analysis also represents that a uniform distribution of 15 ± 5 -nm-diameter gold nanoparticles are deposited on the surface of functionalized GO with a height of 2.6 nm. In addition, the increased values of thickness in RGO-Pr-SH@AuNPs indicate that the process of functionalization has successfully occurred and the functional groups are immobilized on the surface of the RGO. The sample of RGO-Pr-SH@AuNPs exhibits a rougher surface than neat GO. This increase in surface roughness is likely to bind the gold nanoparticles and the adsorption of ions as the solvent evaporates during sample preparation [50].

Fig. 6 TEM image of RGO-Pr-SH@AuNPs



The EDS analysis of the GO and the RGO-Pr-SH@AuNPs catalyst confirmed the presence of organosilane and Au on support (Fig. 8a, b). Also, to support the mentioned observation, the catalyst was subjected to inductively coupled plasma (ICP) analyzer. ICP analysis indicated the presence of Au in the catalyst and the content of Au was estimated to be 2.2 mmol g^{-1} (43%W).

Investigation of catalyst activity of RGO-Pr-SH@AuNPs in the synthesis of tetrahydrobenzo[b]pyrans

The prepared RGO-Pr-SH@AuNPs was used as heterogeneous catalysts in the synthesis of tetrahydrobenzo[b]pyran via the one-pot three-component condensation of various aldehydes, dimedone and malononitrile in water under ultrasound conditions (Scheme 2).

To optimize the reaction conditions, malononitrile, dimedone and 4-chlorobenzaldehyde were selected as a model reaction in the presence of different amounts of catalyst. To observe for optimal solvents, the reaction was tested in various solvents such as H_2O , ethanol, acetonitrile, toluene, and chloroform (Table 1). As shown in Entry 1, the yield of the reaction in water is more than in other solvents. Moreover, the reactions were clean in water compared to those in organic solvents.

In order to obtain the optimal amount of the catalyst, the reaction was carried out in the presence of different amounts of the catalyst (Table 2). The best result was observed when the amount of the catalyst was 3 mg (0.22 mol% Au), and the product yield afforded 97% at 2 min in water under ultrasound irradiations. Also, the reaction was performed in the absence of the catalyst and no product was formed.

As shown in Table 3, we observed the effect of ultrasonic irradiation frequency (range, 20–45 kHz) on the reaction. When the reaction was performed in the absence of ultrasonic irradiation, the product was not obtained at room temperature for 120 min (Table 3, Entry 1), while in the presence of ultrasonic irradiation at a power of 40 kHz and with the RGO-Pr-SH@AuNPs catalyst, the yield increased to 97% after 2 min (Table 3, Entry 4).

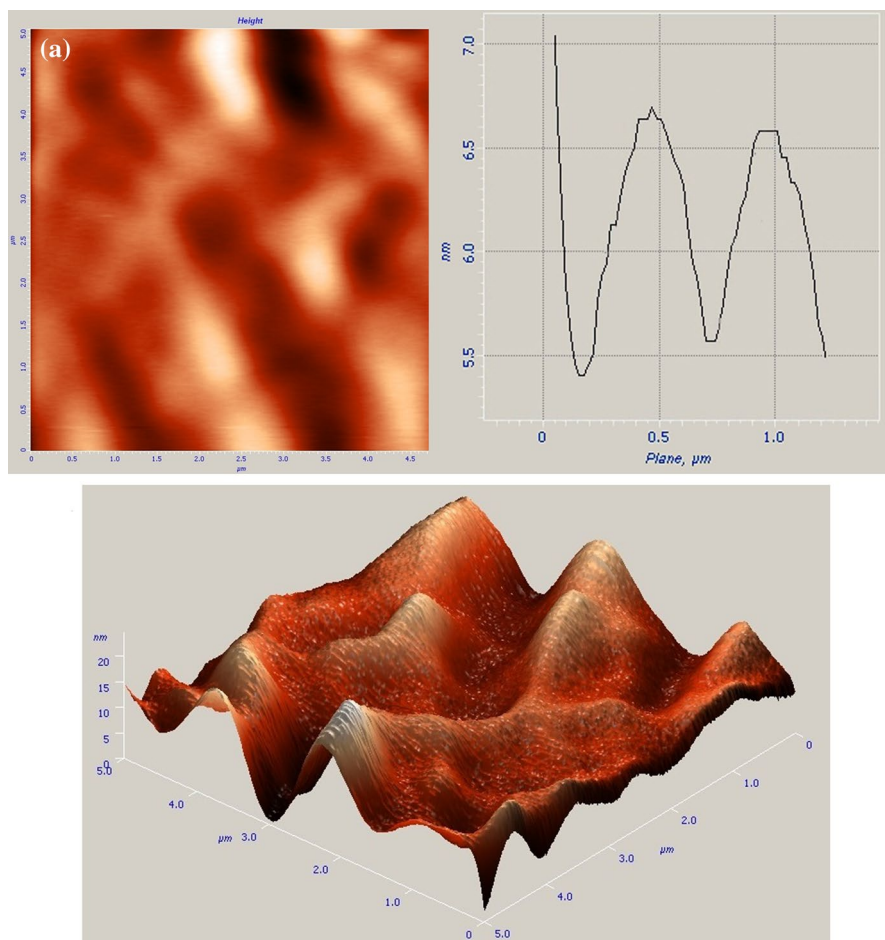


Fig. 7 AFM images of **a** GO nanosheets and **b** RGO-Pr-SH@AuNPs

Therefore, the best results were achieved in water under ultrasonic irradiation with a power of 40 kHz using 3 mg (0.22 mol% Au) of the catalyst. After optimization, we detailed these conditions for a series of different aromatic aldehydes containing electron-releasing and electron-withdrawing substituents to investigate the versatility of the protocol under RGO-Pr-SH@AuNPs catalysis. The results are summarized in Table 4. The results demonstrated that all types of aldehydes were able to render the corresponding products in high yields. Furthermore, the structures of these products were supported by ^1H NMR spectra.

The reusability of the RGO-Pr-SH@AuNPs catalyst was examined in the synthesis of tetrahydrobenzo[b]pyran under optimized conditions. After the end of the reaction, the catalyst was isolated by filtration, washed with EtOH (3×5 mL) and dried at 80 °C in an oven for 24 h. The recycled catalyst could be reused for six

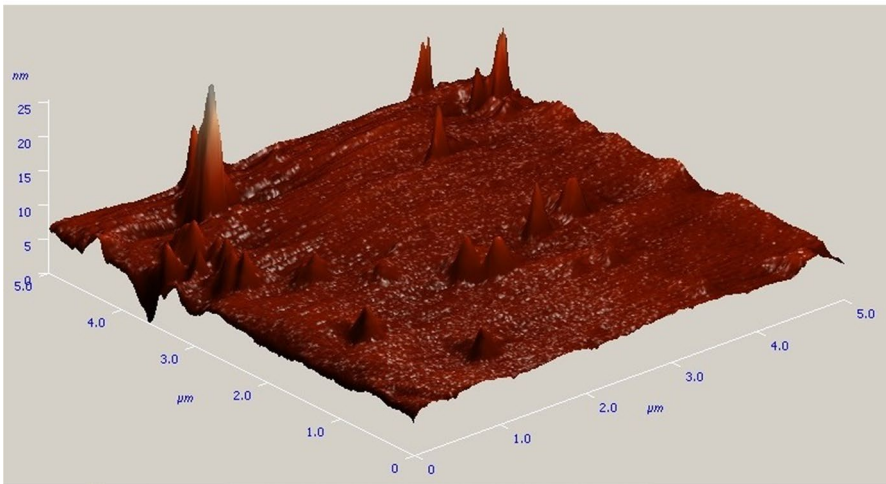
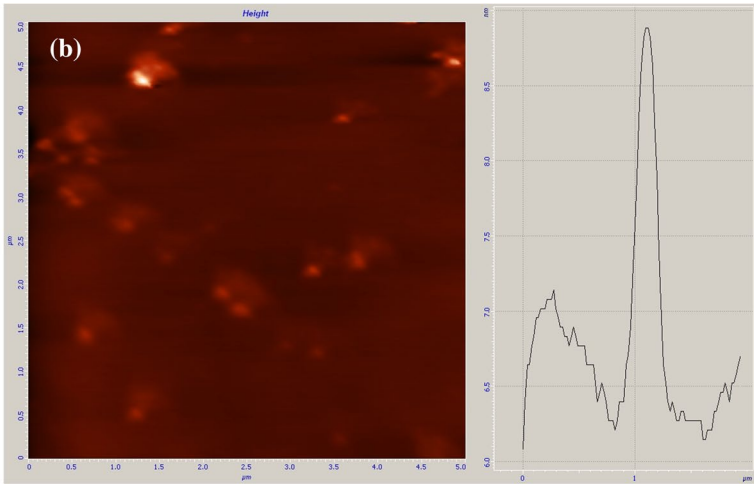


Fig. 7 (continued)

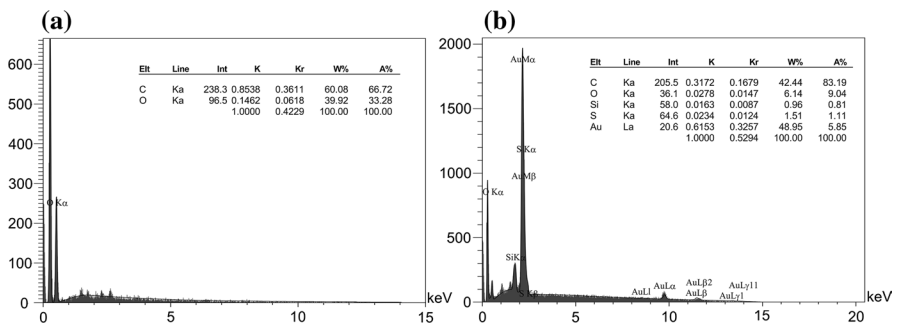
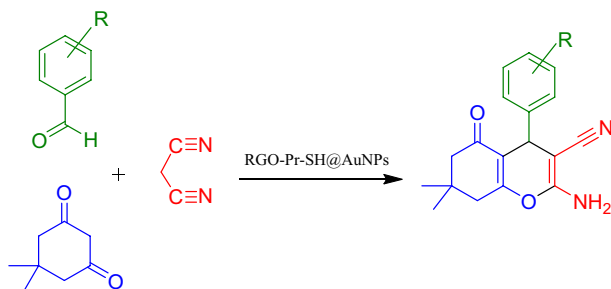


Fig. 8 EDS patterns of a GO and b RGO-Pr-SH@AuNPs



Scheme 2 Synthesis of tetrahydrobenzo[b]pyran

Table 1 Optimization in the presence of different solvents

Entry	Solvent	Time (min)	Yield ^a (%)
1	H ₂ O	2	97
2	EtOH	2	80
3	CH ₃ CN	10	50
4	PhCH ₃	15	35
5	CHCl ₃	10	45

Reaction conditions: dimedone (1 mmol), malononitrile (1 mmol), aldehyde (1 mmol), RGO-Pr-SH@AuNPs (3 mg, 0.22 mol%), under ultrasound conditions

^aIsolated yields

Table 2 Optimization of the RGO-Pr-SH@AuNPs catalyst amount

Entry	Catalyst (mg)	Au (mmol)	Time (min)	Yield ^a (%)
1	0	–	20	–
2	1	0.0022	5	75
3	3	0.0066	2	97
4	5	0.011	2	97

Reaction conditions: dimedone (1 mmol), malononitrile (1 mmol), aldehyde (1 mmol), RGO-Pr-SH@AuNPs, H₂O, under ultrasound conditions

^aIsolated yields

Table 3 Effect of ultrasonic irradiation on the synthesis of tetrahydrobenzo[b]pyran

Entry	US.F (kHz)	Time (min)	Yield ^a (%)
1	Silent	120	–
2	20	10	50
3	30	5	75
4	40	2	97
5	45	2	97

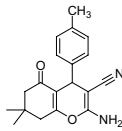
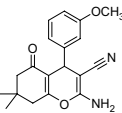
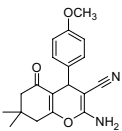
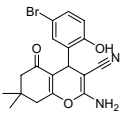
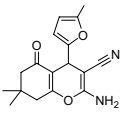
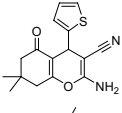
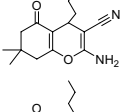
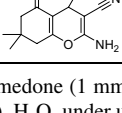
Reaction conditions: conditions: dimedone (1 mmol), malononitrile (1 mmol), aldehyde (1 mmol), H₂O, RGO-Pr-SH@AuNPs (3 mg, 0.22 mol%)

^aIsolated yields

Table 4 Synthesis of tetrahydrobenzo[*b*]pyran catalyzed by RGO-Pr-SH@AuNPs

Entry	Product	<i>T</i> (min)	Yield ^a (%)	TON ^b	TOF ^c (h ⁻¹)
1		10	87	132	776
2		10	85	129	759
3		7	92	139	1158
4		5	95	144	1735
5		2	97	147	4454
6		5	95	144	1735
7		5	93	141	1699
8		2	93	141	4273
9		2	96	145	4394

Table 4 (continued)

Entry	Product	T (min)	Yield ^a (%)	TON ^b	TOF ^c (h ⁻¹)
10		7	87	132	1100
11		7	92	139	1158
12		10	90	136	800
13		10	90	136	800
14		40	92	84	127
15		40	90	82	124
16		120	<10	–	–
17		160	15	–	–

General reaction conditions: dimedone (1 mmol), malononitrile (1 mmol), aldehyde (1 mmol), RGO-Pr-SH@AuNPs (3 mg, 0.22 mol%), H₂O, under ultrasound conditions

^aIsolated yields

^bTON: mole of formed tetrahydrobenzo[b]pyran per mole of catalyst

^cTOF (h⁻¹): (mmol of product/mmol of active site of catalyst)/time of the reaction (h)

times without considerable loss of its catalytic activity and gave the corresponding product in high yields (Fig. 9). Afterwards, the melting point of product was checked to ensure that the purity remained excellent.

The results of this study were compared with some literature reports in order to better display the utility of RGO-Pr-SH@AuNPs in accelerating the reactions under study (Table 5). In each case, the catalyzed reaction with RGO-Pr-SH@AuNPs had

Fig. 9 Reusability of the catalyst RGO-Pr-SH@AuNPs in the synthesis of tetrahydrobenzo[b]pyran

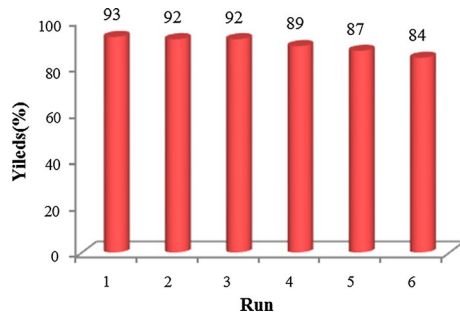


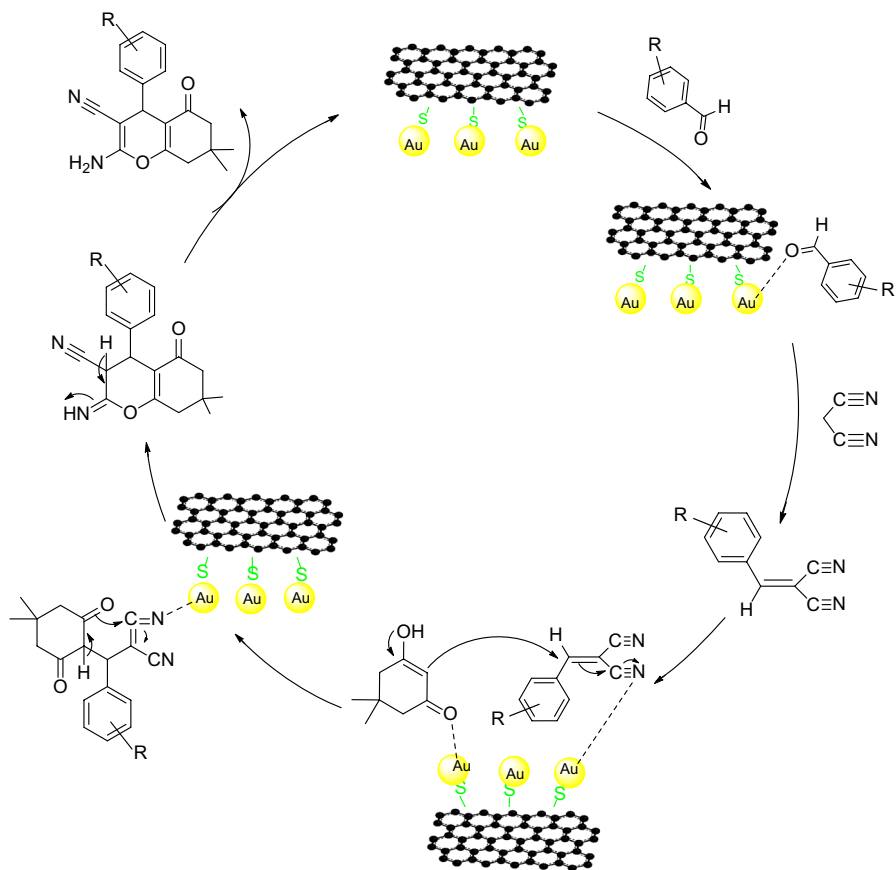
Table 5 Comparison of the catalytic efficiency of RGO-Pr-SH@AuNPs with other catalysts

Catalyst/conditions	Catalyst amount (mol%)	Time (min)	Yield (%)	References
TBABr, EtOH, reflux	10	30	95	[9]
Na ₂ SeO ₄ , EtOH/H ₂ O, reflux	52	180	90	[10]
Taurinea H ₂ O/reflux	28	30	97	[44]
SiO ₂ NPs/r.t./EtOH	5	20	98	[51]
MgO, r.t. H ₂ O	50	15	86	[52]
IRMOF–Zn complex, solvent-free, 60 °C	4	300	90	[53]
[cmmim]Br, solvent-free, 115 °C	10	10	93	[54]
Glycine, H ₂ O, sonication	15	16	92	[55]
RGO-Pr-SH@AuNPs, H ₂ O, sonication	0.22	2	97	Current work

an advantage in applying a nontoxic solvent and a green catalyst, featuring easy separation of product and catalyst, offering catalyst reusability, and resulting in lower reaction times and higher yields.

The proposed reaction mechanism

A plausible mechanism for the synthesis of tetrahydrobenzo[b]pyran using RGO-Pr-SH@AuNPs is shown in Scheme 3. Firstly, RGO-Pr-SH@AuNPs catalyzes the formation of a Knoevenagel intermediate (I) from the reaction of aryl aldehydes and malononitrile (AuNPs are Lewis acidic and so can increase the electrophilicity of the carbonyl group of aryl aldehydes as well as C-H activated compounds). Also, we believe that the cyanide group of intermediate (I) is activated by the RGO-Pr-SH@AuNPs catalyst for nucleophilic attack of dimedone (II) to form a Michael adduct (III). The intermediate (III) undergoes tautomerization and intramolecular cyclization using the RGO-Pr-SH@AuNPs catalyst to form intermediate (IV). Ultimately, after tautomerization of intermediate (IV), tetrahydrobenzo[b]pyran is obtained in high yield and short reaction times.



Scheme 3 Proposed mechanism for the synthesis of tetrahydrobenzo[b]pyran

Conclusion

In this research, we have supported gold nanoparticles on thiol-functionalized reduced GO for a convenient and mild synthesis of tetrahydrobenzo[b]pyrans under ultrasound irradiation. The cooperation between the ultrasound and the nanocatalyst has advantages including high yields in short reaction times and the easy work-up procedures employed. The catalyst was easily recovered and reused six cycles without a significant loss of catalytic activity. Furthermore, the nontoxicity of gold nanoparticles as well as the mild reaction conditions involved makes this an attractive synthetic process from an environmental point of view.

Acknowledgements The authors are grateful to the University of Kashan for supporting this work by Grant Number 159148/79.

References

1. L. Bonsignore, A. De Logu, G. Loy, S. Lavagna, D. Secci, *Eur. J. Med. Chem.* **29**, 479 (1994)
2. N. Hazeri, M.T. Maghsoodlou, F. Mir, M. Kangani, H. Saravani, E. Molashahi, *Chin. J. Catal.* **35**, 391 (2014)
3. A. Saini, S. Kumar, J.S. Sandhu, *Synlett* **2006**, 1928 (2006)
4. L. Tang, J. Yu, Y. Leng, Y. Feng, Y. Yang, R. Ji, *Bioorg. Med. Chem. Lett.* **13**, 3437 (2003)
5. R. Thompson, S. Doggrel, J.O. Hoberg, *Bioorg. Med. Chem.* **11**, 1663 (2003)
6. M. Khoobi, L. Ma'mani, F. Rezazadeh, Z. Zareie, A. Foroumadi, A. Ramazani, A. Shafiee, *J. Mol. Catal. A: Chem.* **359**, 74 (2012)
7. A. Shaabani, S. Samadi, Z. Badri, A. Rahmati, *Catal. Lett.* **104**, 39 (2005)
8. T.-S. Jin, A.-Q. Wang, F. Shi, L.-S. Han, L.-B. Liu, T.-S. Li, *ARKIVOC* **14**, 78 (2006)
9. S. Gurumurthi, V. Sundari, R. Valliappan, *J. Chem.* **6**, S466 (2009)
10. R. Hekmatshoar, S. Majedi, K. Bakhtiari, *Catal. Commun.* **9**, 307 (2008)
11. S. Gao, C.H. Tsai, C. Tseng, C.-F. Yao, *Tetrahedron* **64**, 9143 (2008)
12. Y.-M. Ren, C. Cai, *Catal. Commun.* **9**, 1017 (2008)
13. M.M. Khodaei, K. Bahrami, A. Farrokhi, *Synth. Commun.* **40**, 1492 (2010)
14. S.S. Katkar, M.K. Lande, B.R. Arbad, S.T. Gaikwad, *Chin. J. Chem.* **29**, 199 (2011)
15. D. Azarifar, S.-M. Khatami, R. Nejat-Yami, *J. Chem. Sci.* **126**, 95 (2014)
16. A. Rostami, B. Atashkar, H. Gholami, *Catal. Commun.* **37**, 69 (2013)
17. D. Kumar, V.B. Reddy, B.G. Mishra, R. Rana, M.N. Nadagouda, R.S. Varma, *Tetrahedron* **63**, 3093 (2007)
18. D. Li, M.B. Müller, S. Gilje, R.B. Kaner, G.G. Wallace, *Nat. Nanotechnol.* **3**, 101 (2008)
19. Y. Yıldız, S. Kuzu, B. Sen, A. Savk, S. Akocak, F. Şen, *Int. J. Hydrog. Energy* **42**, 13061 (2017)
20. B. Çelik, G. Başkaya, H. Sert, Ö. Karatepe, E. Erken, F. Şen, *Int. J. Hydrog. Energy* **41**, 5661 (2016)
21. Y. Yıldız, E. Erken, H. Pamuk, H. Sert, F. Şen, *J. Nanosci. Nanotechnol.* **16**, 5951 (2016)
22. E. Demir, A. Savk, B. Sen, F. Sen, *Nano Struct. Nano Objects* **12**, 41 (2017)
23. Z. Daşdelen, Y. Yıldız, S. Eriş, F. Şen, *Appl. Catal. B* **219**, 511 (2017)
24. S. Akocak, B. Şen, N. Lolak, A. Şavk, M. Koca, S. Kuzu, F. Şen, *Nano Struct. Nano Objects* **11**, 25 (2017)
25. H. Naeimi, M. Golestanzadeh, *RSC Adv.* **4**, 56475 (2014)
26. B. Aday, H. Pamuk, M. Kaya, F. Sen, J. Nanosci. Nanotechnol. **16**, 6498 (2016)
27. Y. Yıldız, T.O. Okyay, B. Sen, B. Gezer, S. Kuzu, A. Savk, E. Demir, Z. Dasdelen, H. Sert, F. Sen, *ChemistrySelect* **2**, 697 (2017)
28. R. Ayrançi, G. Başkaya, M. Güzel, S. Bozkurt, F. Şen, M. Ak, *ChemistrySelect* **2**, 1548 (2017)
29. S. Bozkurt, B. Tosun, B. Sen, S. Akocak, A. Savk, M.F. Ebeoğlugil, F. Sen, *Anal. Chim. Acta* **989**, 88 (2017)
30. N. Yan, C. Xiao, Y. Kou, *Coord. Chem. Rev.* **254**, 1179 (2010)
31. H. Goksu, Y. Yıldız, B. Çelik, M. Yazici, B. Kilbas, F. Sen, *Catal. Sci. Technol.* **6**, 2318 (2016)
32. C. Shen, C. Hui, T. Yang, C. Xiao, J. Tian, L. Bao, S. Chen, H. Ding, H. Gao, *Chem. Mater.* **20**, 6939 (2008)
33. K. Datta, B. Reddy, K. Ariga, A. Vinu, *Angew. Chem. Int. Ed.* **49**, 5961 (2010)
34. B. Zhu, M. Lazar, B.G. Trewyn, R.J. Angelici, *J. Catal.* **260**, 1 (2008)
35. C. Marsden, E. Taarning, D. Hansen, L. Johansen, S.K. Klitgaard, K. Egeblad, C.H. Christensen, *Green Chem.* **10**, 168 (2008)
36. Y. Tai, J. Murakami, K. Tajiri, F. Ohashi, M. Daté, S. Tsubota, *Appl. Catal. A* **268**, 183 (2004)
37. G. Li, D.-E. Jiang, C. Liu, C. Yu, R. Jin, *J. Catal.* **306**, 177 (2013)
38. P. Garcia, M. Malacria, C. Aubert, V. Gandon, L. Fensterbank, *ChemCatChem* **2**, 493 (2010)
39. H. Naeimi, Z. Ansarian, *Inorg. Chim. Acta* **466**, 417 (2017)
40. M. Nasrollahzadeh, A. Ehsani, A. Rostami-Vartouni, *Ultrason. Sonochem.* **21**, 275 (2014)
41. M. Dabiri, Z.N. Tisseh, M. Bahramnejad, A. Bazgir, *Ultrason. Sonochem.* **18**, 1153 (2011)
42. H. Zang, Q. Su, Y. Mo, B.-W. Cheng, S. Jun, *Ultrason. Sonochem.* **17**, 749 (2010)
43. G. Cravotto, P. Cintas, *Chem. Soc. Rev.* **35**, 180 (2006)
44. F. Shirini, N. Daneshvar, *RSC Adv.* **6**, 110190 (2016)
45. S. Rostamnia, A. Nuri, H. Xin, A. Pourjavadi, S.H. Hosseini, *Tetrahedron Lett.* **54**, 3344 (2013)
46. L.-M. Wang, J.-H. Shao, H. Tian, Y.-H. Wang, B. Liu, *J. Fluor. Chem.* **127**, 97 (2006)
47. P.K. Paliwal, S.R. Jetti, S. Jain, *Med. Chem. Res.* **22**, 2984 (2013)

48. Y. Zhou, Q. Bao, L.A.L. Tang, Y. Zhong, K.P. Loh, *Chem. Mater.* **21**, 2950 (2009)
49. P. Cui, S. Seo, J. Lee, L. Wang, E. Lee, M. Min, H. Lee, *ACS Nano* **5**, 6826 (2011)
50. I.V. Lightcap, T.H. Kosel, P.V. Kamat, *Nano Lett.* **10**, 577 (2010)
51. S. Banerjee, A. Horn, H. Khatri, G. Sereda, *Tetrahedron Lett.* **52**, 1878 (2011)
52. D. Kumar, V.B. Reddy, S. Sharad, U. Dube, S. Kapur, *Eur. J. Med. Chem.* **44**, 3805 (2009)
53. S. Rostamnia, A. Morsali, *Inorg. Chim. Acta* **411**, 113 (2014)
54. A.R. Moosavi-Zare, M.A. Zolfigol, O. Khaledian, V. Khakyzadeh, M.D. Farahani, H.G. Kruger, *New J. Chem.* **38**, 2342 (2014)
55. B. Datta, M. Pasha, *Ultrason. Sonochem.* **19**, 725 (2012)